Automated assessment of mandibular shape asymmetry in 3-dimensions

Yi Fan,[a] Yungeng Zhang,[b] Gui Chen,[c] Wei He,[d] Guangying Song,[c] Harold Matthews,[e] Peter Claes,[f] Yuru Pei,[b] Hongbin Zha,[b] Anthony Penington,[g] Nicky Kilpatrick,[g] Paul Schneider,[h] Ruoping Jiang,[c] and Tianmin Xu[c]
Beijing, China, Melbourne, Australia, and Leuven, Belgium

Introduction: This study aimed to develop an automatic pipeline for analyzing mandibular shape asymmetry in 3-dimensions. **Methods:** Forty patients with skeletal Class I pattern and 80 patients with skeletal Class III pattern were used. The mandible was automatically segmented from the cone-beam computed tomography images using a U-net deep learning network. A total of 17,415 uniformly sampled quasi-landmarks were automatically identified on the mandibular surface via a template mapping technique. After alignment with the robust Procrustes superimposition, the pointwise surface-to-surface distance between original and reflected mandibles was visualized in a color-coded map, indicating the location of asymmetry. The degree of overall mandibular asymmetry and the asymmetry of subskeletal units were scored using the root-mean-squared-error between the left and right sides. These asymmetry parameters were compared between the skeletal Class I and skeletal Class III groups. **Results:** The mandible shape was significantly more asymmetrical in patients with skeletal Class III pattern with positional asymmetry. The condyles were identified as the most asymmetric region in all groups, followed by the coronoid process and the ramus. **Conclusions:** This automated approach to quantify mandibular shape asymmetry will facilitate high-throughput image processing for big data analysis. The spatially-dense landmarks allow for evaluating mandibular asymmetry over the entire surface, which overcomes the information loss inherent in conventional linear distance or angular measurements. Precise quantification of the asymmetry can provide important information for individualized diagnosis and treatment planning in orthodontics and orthognathic surgery. (Am J Orthod Dentofacial Orthop 2022;161:698-707)

The mandible is the primary moving and functioning bone in the craniofacial skeleton and plays a central role in determining facial morphology and esthetics.[1] Facial asymmetry can be caused by a discrepancy in the size and shape of the 2 halves of the mandible (shape asymmetry) or by a misalignment between the midface and the mandible (positional asymmetry). Shape asymmetry of the mandible is a common craniofacial deformity that occurs in a diverse set of congenital and acquired conditions such as craniofacial microsomia, trauma, fracture, arthritis, or infection of the temporomandibular joints.[2,3] An asymmetrically shaped mandible could coexist with the positional asymmetry of the

[a]Department of Orthodontics, Peking University School and Hospital of Stomatology, and National Engineering Laboratory for Digital and Material Technology of Stomatology, Beijing Key Laboratory of Digital Stomatology, Peking University School and Hospital of Stomatology, Beijing, China; Facial Science, Murdoch Children's Research Institute, Melbourne, Australia.
[b]Key Laboratory of Machine Perception (MOE), Department of Machine Intelligence, Peking University, Beijing, China.
[c]Department of Orthodontics, Peking University School and Hospital of Stomatology, and National Engineering Laboratory for Digital and Material Technology of Stomatology, Beijing Key Laboratory of Digital Stomatology, Peking University School and Hospital of Stomatology, Beijing, China.
[d]Department of Oral and Maxillofacial Surgery, Peking University School and Hospital of Stomatology, Beijing, China.
[e]Facial Science, Murdoch Children's Research Institute, Melbourne, Australia; Department of Human Genetics, KU Leuven, and Medical Imaging Research Centre, Universitair Ziekenhuis, Leuven, Belgium.
[f]Facial Science, Murdoch Children's Research Institute, Melbourne, Australia; Department of Human Genetics and Department of Electrical Engineering, KU Leuven, and Medical Imaging Research Centre, Universitair Ziekenhuis, Leuven, Belgium.
[g]Facial Science, Murdoch Children's Research Institute, and The University of Melbourne, Department of Paediatrics at the Royal Children's Hospital, Melbourne, Australia.
[h]The University of Melbourne Dental School, Orthodontics, Melbourne, Australia.
All authors have completed and submitted the ICMJE Form for Disclosure of Potential Conflicts of Interest, and none were reported.
This work was supported by National Natural Science Foundation (82001091 and 82071172), Beijing Municipal Science & Technology Commission (Z181100001718112), and EA-PKU Specialized Programs of Research Excellence on Clear Aligner Treatment (B4-WXEA2012361).
Address correspondence to: Ruoping Jiang, Department of Orthodontics, Peking University School and Hospital of Stomatology, 22 Zhongguancun South Ave, Haidian District, Beijing 100081, China; e-mail, jiangruoping@126.com and Tianmin Xu, Department of Orthodontics, Peking University School and Hospital of Stomatology, 22 Zhongguancun South Ave, Haidian District, Beijing 100081, China; e-mail, tmxuortho@163.com.
Submitted, April 2021; revised and accepted, July 2021.
0889-5406/$36.00

https://doi.org/10.1016/j.ajodo.2021.07.014

mandible. Imbalanced occlusion and abnormal stress distribution on the articular surface could affect the condylar modeling during the active growth period.[4] Alternatively, the unpredictable nature of growth can result in progressive mandibular shape deformity with age.

Detecting and quantifying asymmetry is important to clinicians, facilitating more accurate differentiation and diagnosis of the causes of asymmetry and more effective treatment planning. Traditionally, posteroanterior cephalograms and submentovertex radiographs are taken to determine the presence and degree of the mandibular asymmetry.[5,6] In the classic triangulation method, the left side and right side of the mandible are simplified as the triangles between the condylar point, gonion, and menton, then the shape asymmetry is measured as the difference between the 2 sides.[7] Others evaluate the mandibular asymmetry using a reference midline. A reference midline is often generated by connecting median landmarks or bisecting the lines connecting bilateral landmarks of the midface. Differences are compared between pairwise corresponding linear distances perpendicularly to the reference midline.[8,9] In general, landmark placement is difficult in 2-dimensional (2D) planes because spatially separate structures are projected onto overlapping positions in the 2D image plane. Manual landmarking is laborious and requires a skilled operator with anatomic knowledge. Interoperator and intraoperator landmarking variability are important sources of error and inconsistency in linear distance or angle measurements. Moreover, the rotation of the mandible relative to the 2D image plane will adversely affect the measurement of the morphologic asymmetry. This makes the positional and morphologic asymmetry of the mandible challenging to disentangle from a 2D radiograph.[10]

Computed tomography, either spiral computed tomography or cone-beam computed tomography (CBCT), offers greater precision in measuring craniofacial structures in 3-dimensions (3D). However, the deformity of the mandible has often been summarized as the difference in distances, angles, area, or ratio between the left and right sides of the jaw.[11,12] Arguably, these do not accurately represent the complex structure of the mandible. In addition, the reproducibility in identifying landmarks in smooth structures such as the condyle is considered a major source of errors in these analyses. Different landmark choices could lead to contrasting outcomes.[13] Furthermore, as big data initiatives become increasingly common in dentistry and surgical disciplines, there is pressure to develop fast, automatic, and standardized measurements for patient evaluation in this field.

Therefore, this study aimed to develop an automatic pipeline for mandibular shape asymmetry assessment. This comprises automatically segmenting the mandible from CBCT images, identifying spatially-dense landmarks on the mandibular surface, and comparing original and reflected copies of the images to determine the asymmetry (Fig 1). We illustrate this method by comparing the mandibular shape asymmetry between adults with the skeletal Class I pattern with those with the skeletal Class III pattern.

MATERIAL AND METHODS

The patients were retrospectively collected at the Department of Orthodontics at Peking University School of Stomatology from 2015-2018. We selected 120 adult subjects (aged >18 years) whose CBCT scans were taken for clinical indications. The patients were divided into skeletal Class I group (40 subjects; mean age, 20.32 ± 3.78 years) and skeletal Class III group (80 subjects; mean age, 21.20 ± 4.65 years) on the basis of the ANB angle (normal value, 2.7°; standard deviation, 2.0°). Patients were further divided by the positional asymmetry of the mandible, which was defined by manually measuring the distance from the hard-tissue menton point to the midsagittal reference plane in the CBCT images.[14] A distance between the midsagittal reference plane and skeletal menton >4 mm was taken as an indication of the positional asymmetry of the mandible. Finally, 3 subgroups were constituted. Group 1: patients with skeletal Class I pattern without positional asymmetry (n = 40); group 2: patients with skeletal Class III pattern without positional asymmetry (n = 40); and group 3: patients with skeletal Class III pattern with positional asymmetry (n = 40). The following criteria also had to be fulfilled: (1) Chinese ethnicity; (2) no multiple missing teeth other than third molars; and (3) no congenital diseases affecting growth and development, no previous craniofacial surgery, facial fractures or facial surgery, degenerative disease in the temporomandibular joint, and craniofacial anomalies. Ethical approval was obtained from the Research Ethics Committee of the Peking University School and Hospital of Stomatology (PKUSSIRB-202057109). Written informed consent was obtained from all participants.

All the CBCT scans were obtained from the same device (NewTom 9000; Quantitative Radiology, Verona, Italy). Patients were instructed to sit naturally upright, close their mouths in maximum intercuspation, and relax their lips. The field of view in the selected samples was 16 × 13 cm or 17 × 23 cm with a scan time 18.0-26.9 seconds. Exposure parameters for CBCT images were 120 kVp and 3-8 mA. The original isotropic voxel size was 0.5 mm^3.

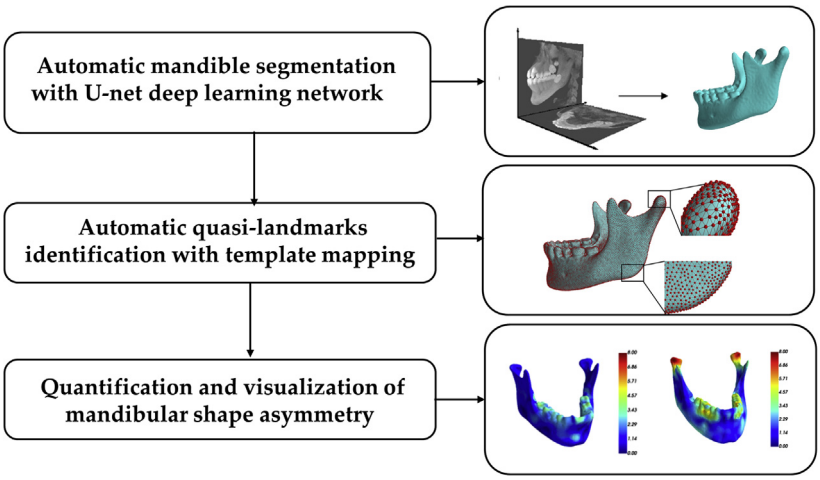

Fig 1. The automated mandibular shape asymmetry assessment pipeline.

The mandible was segmented from each CBCT image using a 3D U-net architecture, a deep-learning-based automatic segmentation approach.[15] The framework of the automatic segmentation is shown in Figure 2. Briefly, the segmentation network was trained using 48 segmented CBCT images. For these 48 images, segmentation was performed with ITK-SNAP open-source software case by case (http://www.itksnap.org/pmwiki/pmwiki.php).[16,17] It requires an initial segmentation using global thresholding to grossly segment the main part mandible, followed by a selection of seed points and a "region competition snake" algorithm to generate the region of interest, such as the condyles.

For the automatic segmentation approach, the original CBCT images were cropped into patches of 192 × 192 × 192 in the training and inference stage because of the limitation of graphics processing unit memory. The network had an encoder-decoder structure with long skip connections. The encoder compressed the image patch into feature maps in low resolution, and the decoder aimed to estimate a probability at each voxel that it belongs to the mandible. In this study, the encoder had 5 ResNet-like blocks, each followed by a 2 × 2 × 2 average pooling layer. The decoder had 4 ResNet-like blocks and two 3 × 3 × 3 convolutional layers, followed by an upsampling layer. Each ResNet block consisted of two 3 × 3 × 3 convolutional layers for feature extraction and one 1 × 1 × 1 convolutional layer for residual connection. The instance normalization layer and Leaky ReLU activation followed each convolutional layer. The feature volumes in the decoder stage were composed of volumes from the proceeding layers in the decoder and those from the encoder with the same resolution. The output of the decoder was the mandible segmentation of patches. We used a cross-entropy loss function to train the segmentation network. In the inference stage, the mandible segmentation of patches from each CBCT image was merged to get the final mandible segmentation. The overlapping sliding window method was used to crop patches with a stride of 60 × 60 × 60. For the overlapping areas, we used the average probability of each voxel belonging to the mandible to get the final mandible prediction. The segmentation network was implemented using the open-source PyTorch.

The ITK-SNAP software is open-source, and the framework of the proposed automatic method is implemented using an open-source convolutional neural network, and thereby both are free. The time efficiency and the accuracy of the automatic mandible segmentation approach were further compared. Twenty new CBCT images were used for the validation test. The ITK-SNAP segmented result was considered as a ground truth. The ITK-SNAP and automatically segmented mandibles were compared using the Dice similarity coefficient, which assesses to what degree the same voxels are selected by each segmentation. This index ranges from 0 (no overlap) to 1 (complete overlap). The Average Hausdorff Distance was used to evaluate the discrepancy between the outer surfaces of the mandibles segmented using each approach.

The outer surface of the mandible was tessellated with the standard marching cubes technique in MATLAB software (https://www.mathworks.cn/help/matlab/ref/isosurface.html). Each mandible was then represented by a surface mesh composed of a dense cloud of points linked to define the mandibular surface.

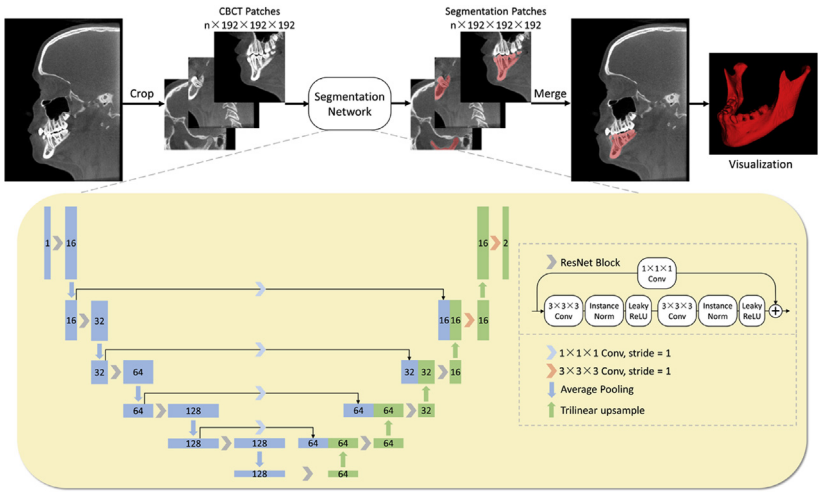

Fig 2. Mandible segmentation framework. *Conv*, Convolution layer.

A previously developed open-source template mapping technique was used to automatically identify spatially-dense quasi-landmarks on the mandibular surface.[18] Essentially, a generic mandibular template was represented by 17,415 quasi-landmarks; these landmarks were defined by x-, y-, and z-coordinates. The template was translated, rotated, and scaled (rigid registration) to roughly align to each target mandible. Then, the template was deformed into the shape of each mandible via a nonrigid registration.[19,20] This procedure ensured that a large number of quasi-landmarks cover the entire surface of the bone, including discrete areas such as the ramus, the condyles, and chin, in which traditional anatomic landmarks are poorly defined by local geometry. After template mapping, each quasi-landmark was a single measurement in a specific anatomic location of the mandible and was in spatial correspondence across all patients (Fig 3). The reflected mandible was generated by reversing the sign of the x-coordinate of each vertex for the original mandible, which generated a reversed 3D image of the entire mandible. This reflected mandible was registered by the same template mapping procedure. The accuracy and reproducibility of the template mapping have been recently validated by Verhelst et al.[21] The average Euclidean distance between manual and corresponding automatic landmarks was 1.40 mm for unaltered and 1.76 mm for operated mandibles, respectively. The variation among repeated mappings was 0.0067 mm and 0.0077 mm for pre and postoperative samples, respectively.[21]

Shape asymmetry of the mandible was assessed by superimposing it onto its reflected version using a robust Procrustes alignment. The discrepancy between corresponding quasi-landmarks of the 2 configurations indicated where the asymmetry occurred. The difference at each quasi-landmark was projected onto the original configuration and graphically visualized by a color map in millimeters. This indicated the location and magnitude of the mandibular shape asymmetry for each patient.

An overall asymmetry index was obtained by calculating the root-mean-squared error between superimposed landmarks of the original and reflected configurations. Teeth were cut off based on the correspondence so that only the nondental component of the mandibular asymmetry was evaluated. Different mandibular regions, including the chin, mandibular body, ramus, condyle, and coronoid process, were further defined on the template by a modified method of Duran et al[14] (Fig 4). The asymmetry indexes of these regions were further calculated to assess the regional asymmetry. All the analyses were implemented using custom-written code in the Python programming language. The overall asymmetry index and the asymmetry indexes of mandibular regions were compared among 3 subgroups using the Kruskal-Wallis H-test via IBM SPSS statistical software (version 23.0; IBM, Armonk, NY). At $P < 0.05$, the difference was considered significant.

RESULTS

Automatic segmentation of each mandible executed in 12-30 seconds on an NVIDIA GTX TITAN XP GPU (Nvidia Corporation, Santa Clara, Calif). The compared ITK-SNAP method typically required 15 to 20 minutes.

Mandibles segmented from the proposed automated method were compared against the ITK-SNAP segmentation method. The Dice similarity coefficient was

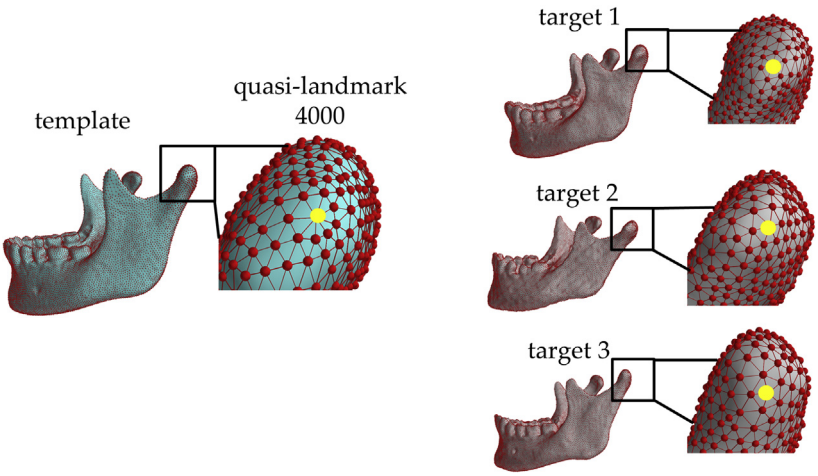

Fig 3. The mandible is represented by spatially-dense quasi-landmarks on the mandibular surface. After the template mapping, each quasi-landmark occupied the same position on a given mandible as on all the other mandibles.

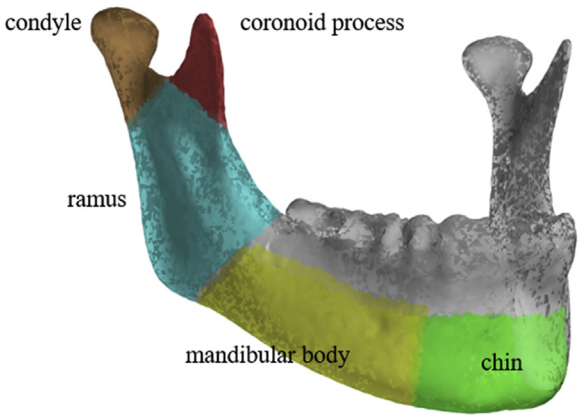

Fig 4. The 5 mandibular regions defined on the template.

0.969 ± 0.005, and the Average Hausdorff Distance was 0.035 ± 0.040 (mm), indicating almost complete overlap between the automatically segmented mandibles and the ITK-SNAP segmented mandibles. Boundary deviations were predominantly <1 mm over the mandibular surfaces (Fig 5).

The overall mandibular asymmetry index and regional indexes were higher in the skeletal Class III group with positional asymmetry. All differences were statistically significant. Condyles have been identified as the main sites of the asymmetric regions in all groups, followed by the coronoid process and the ramus (Table).

The quantification and visualization effects were plotted in 6 selected patients, indicating the region and severity of the mandibular shape asymmetry for patient-based analysis (Fig 6).

DISCUSSION

Objective and precise quantification of the mandibular asymmetry is essential to understand the etiology of the asymmetry and formulate personalized treatment plans. This study describes an automatic method of assessing mandibular shape asymmetry. We automatically segment the mandible from CBCT images with a deep learning U-net architecture and identify spatially-dense quasi-landmarks on the mandibular surface. This facilitates the objective assessment of asymmetry in the shape of the mandible. We illustrate this pipeline by comparing the shape asymmetry of the mandible between patients with skeletal Class I pattern and skeletal Class III pattern. We have demonstrated that the mandible shape is significantly more asymmetrical in patients with skeletal Class III patterns with positional asymmetry. Furthermore, the condyle has been shown to be the most asymmetric site across all groups. Compared with conventional linear distance or angular measurements, the proposed pipeline allows for quantification and visualization of the asymmetric features of the mandible across the entire surface and provides intuitive and objective diagnostic information to clinicians.

Mandibular asymmetry is more likely to occur in patients with skeletal Class III pattern in our sample, consistent with findings in other ethnic populations.[22] The mandible has a longer growth period and is not rigidly connected to the skull base, as is the maxilla.[12] The asymmetry occurs in patients with skeletal Class III pattern with positional asymmetry of the mandible possibly because of excessive mandibular growth under unbalance pressure.[23] By analyzing the subskeletal

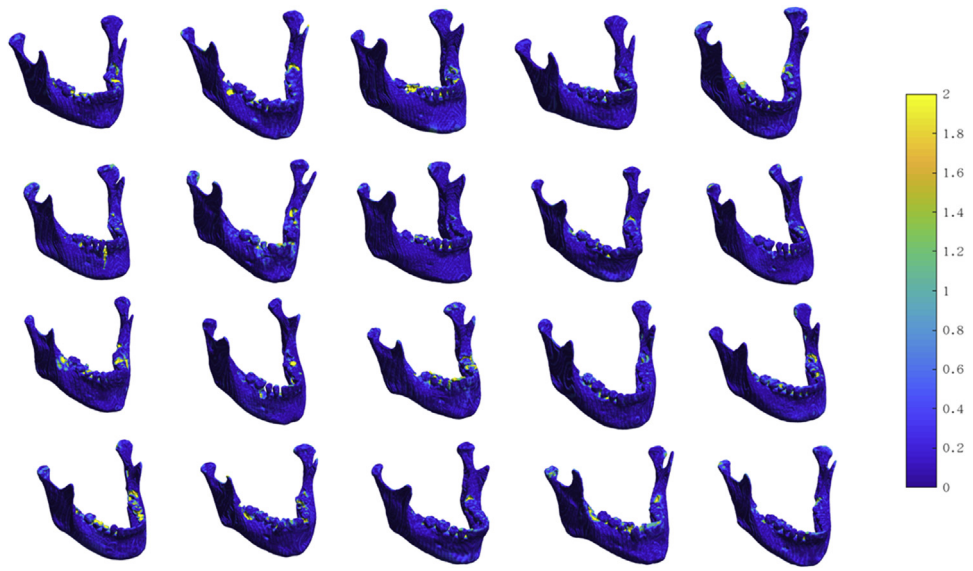

Fig 5. The discrepancy between the proposed automatic method and the ITK-SNAP method in 20 test patients. The color *dark blue* indicates there is no discrepancy between the 2 methods.

units, the condyle was found to be the most asymmetric region in all groups, with greater severity in patients with skeletal Class III patterns. This perhaps further influences the height of the mandibular ramus. The intuitive visualization of this method allows the asymmetry to be presented in a way that directly relates to the morphology of the structure being studied. This is useful to capture subtle but important changes that are difficult to define using traditional linear distance or angular measurement and could also be beneficial for clinician-patient communication. In addition, optimal treatment outcomes are primarily based on precise recognition of the categories of the asymmetry. For instance, surgical procedures such as osteotomies, bone segment relocation, or bone graft insertion are useful for shape asymmetry correction, whereas both orthodontic treatment and orthognathic surgery could correct positional asymmetry to a different extent. The proposed method differentiates the 2 categories of mandibular asymmetry, which could provide intuitive guidance for more precise and objective treatment plans.

Previous studies rely on panoramic radiographs or anteroposterior radiographs to evaluate mandibular shape asymmetry,[24] both of which are subject to errors that arise from magnification differences, geometric distortion, positioning of the head, and overlaying of anatomic structures. Today, evaluating the entire mandibular geometry in 3D creates the opportunity for a more comprehensive and accurate assessment of the complex craniofacial feature as a whole. However, several factors hinder the development of a large number of patient measurements, such as tedious and time-consuming bone segmentation and landmark indication procedures.

Segmenting the mandible from a CBCT image of the head is usually performed by software such as Mimics (Materialise, Leuven, Belgium), Dolphin Imaging (Dolphin Imaging and Management Solutions, Chatsworth, Calif), InVivoDental (Anatomage, San Jose, Calif), or open-source ITK-SNAP software.[16,17] This is operator-dependent and must be done on a case-by-case basis. Automated approaches are therefore desirable. Traditional methods such as deformable volumetric image registration techniques rely on nonlinear iterative optimization to establish the voxel-wise correspondence.[25] Concerning the large set of parameters to be estimated, this solution is computationally intensive. Other approaches such as statistical shape models,[26] multi-atlas label registration,[27] or machine learning[28] require the collection of large amounts of manually segmented mandibles as training data, which may be impractical in real situations.

In this work, we used a supervised U-net deep learning framework to segment the mandible from CBCT images. This solution has several advantages: first, only a few labeled images are required to train a network. These images could be augmented with various techniques (such as flip and affine transformation), thus generating a reliable automatic segmentation network.

Table. Mandibular asymmetry comparison between patients with skeletal Class I and skeletal Class III patterns

Variables	*G1: Patients with skeletal Class I pattern without positional asymmetry*		*G2: Patients with skeletal Class III pattern without positional asymmetry*		*G3: Patients with skeletal Class III pattern with positional asymmetry*		*P values*			
	Median (IQR)	*Min-Max*	*Median (IQR)*	*Min-Max*	*Median (IQR)*	*Min-Max*	*G1-G2-G3*	*G1-G2*	*G2-G3*	*G1-G3*
Overall AI	1.51 (1.28-1.90)	0.86-3.74	1.62 (1.36-2.05)	0.91-4.96	3.24 (2.56-4.05)	1.13-6.31	<0.001**	0.871	<0.001**	<0.001**
Condylar AI	2.14 (1.86-3.03)	0.82-6.85	2.27 (1.70-3.41)	1.05-12.95	6.77 (4.72-8.88)	1.66-13.13	<0.001**	>0.999	<0.001**	<0.001**
Coronoid process AI	1.78 (1.24-2.38)	0.80-3.23	1.95 (1.27-2.80)	0.85-3.72	2.97 (2.26-3.94)	0.81-7.95	<0.001**	0.677	<0.001**	<0.001**
Ramus AI	1.53 (1.26-2.07)	0.83-3.13	1.57 (1.37-3.21)	1.68-2.78	2.62 (2.19-3.27)	1.55-5.64	<0.001**	>0.999	<0.001**	<0.001**
Mandibular body AI	1.53 (1.26-2.07)	1.26-3.13	1.42 (1.04-1.68)	0.81-2.96	1.93 (1.43-2.40)	1.03-3.88	<0.001**	0.183	<0.001**	<0.001**
Chin AI	1.01 (0.76-1.38)	0.68-3.76	1.29 (0.90-1.56)	0.61-3.31	2.43 (1.79-3.18)	1.02-6.08	<0.001**	0.197	<0.001**	<0.001**

Note. Group difference was determined using Kruskal-Wallis H-test.
IQR, interquartile range (25th, 75th percentile); *Min*, minimum; *Max*, maximum; *AI*, asymmetry index.
** $P < 0.001$.

Second, because of the limitation of graphics processing unit memory, a convolutional neural network cannot process the original high-resolution CBCT image in a single forward propagation, whereas patch-based segmentation procedure endows the framework with the ability to segment high-resolution CBCT images. Third, this fully automated setup is computationally efficient, requiring only 12-30 seconds to segment one mandible from a CBCT image.

Another benefit of this asymmetry assessment pipeline is treating the mandible as shape per se instead of extracting linear or angular parameters from the entire structure. In the early days, shape-analysis-based methods of assessing asymmetry were applied to various craniofacial structures. Ercan et al[29] evaluated facial asymmetry in young, healthy subjects by Euclidean distance matrix analysis. This method calculated all possible linear distances among 42 facial landmarks. Then any differences between the right side and left side of the face were compared. Ferrario et al[30] assessed the asymmetry of mandibular and maxillary arches on the basis of 47 homologous points. These landmarks cover more features of the complex anatomic structures, thus preserving more information than conventional measurements. However, these require manual digitalization of a large number of landmarks on the images. Moreover, these studies present the findings as summarized linear distances statistics, which are not easily interpreted by clinicians. These have contributed to a general disillusionment in the dental research community with the shape-analysis-based approach and the continued focus on linear and angular measurements.

In contrast, we perform asymmetry analysis on the basis of thousands of quasi-landmarks automatically identified on the mandibular surface in this study. The procedure is automatic and thus highly reproducible. Moreover, quasi-landmark correspondence is used rather than the traditionally more well-known closest-point correspondence when superimposing the original mandible onto the reflected version. The closest-point correspondence is incorrect when dealing with severely asymmetric patients.[31,32] In a mandible such as that shown in Figure 7, in which the length of the ramus on one side is longer than the other, superimposing the long ramus and the short ramus with the iterative closest-point algorithm leads to anatomically meaningless correspondence between the 2 sides of the condyles (Fig 7, *B*). The template mapping also incorporates closest-point correspondence but with closest points updated as the template changes its shape. This ensures anatomically meaningful correspondence is established at the end of the algorithm. For example, the condylion point on the long ramus side corresponds to the

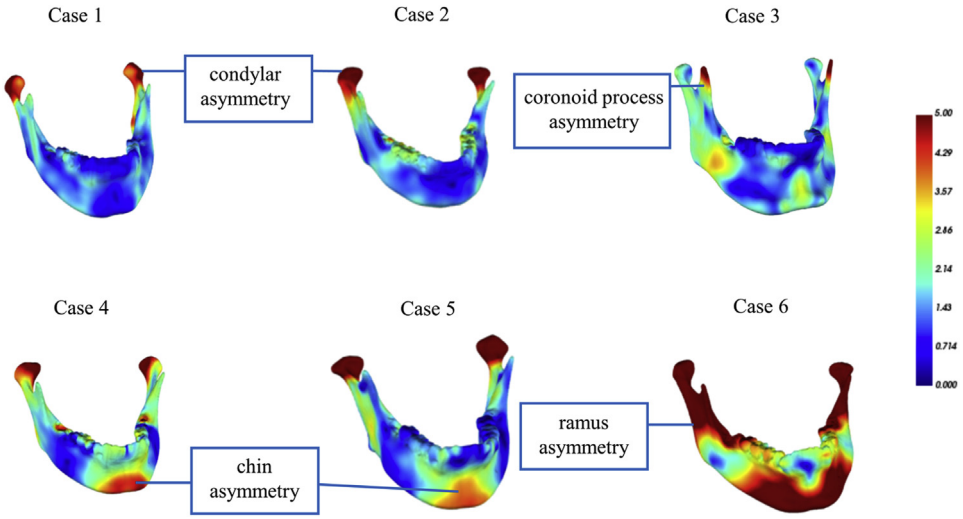

Fig 6. Shape asymmetry of the mandibles varies from patient to patient. *Red* areas indicate regions in which the asymmetry was >4 mm, and *dark blue* indicate no asymmetry.

condylion point on the short ramus side of the mandible (Fig 7, *A*). After superimposing the 2 surface meshes, the accuracy of the correspondences determined the accuracy of color map visualizations and derived asymmetry indexes.

Efficient and powerful computer-based medical image processing techniques are highly valued in the era of big data. In general, the proposed pipeline addresses 3 aspects of clinical assessment. (1) Time and resources can be saved by streamlining and automating mandibular segmentation, landmark indication, and asymmetry measurement. They allow large numbers of images to be analyzed in standardized, fast, and objective ways; (2) by measuring asymmetry across the whole surface of the mandible, we improve on more traditional methods on the basis of sparsely annotated landmarks or interlandmark distances; (3) although the proposed method whereby asymmetry is assessed across the whole surface, our approach substantially improves the asymmetry assessment accuracy in especially in patients with extreme asymmetry. We believe that many clinicians will be interested in technical aspects of the method as image analysis methods become more incorporated into orthodontic practice.

The limitation of this study is that the proposed technique is not clinician-friendly and requires basic coding knowledge. However, cross-disciplinary collaborations between clinical departments and computer scientists are becoming more common. Advanced image analysis methods, focusing on how they can benefit the clinical community, are valuable as the ultimate goal is to save time and resources for clinicians and improve patient assessment and patient care. Future endeavors should make this pipeline an open-source tool with a user-friendly interface. Furthermore, we illustrate an automated pipeline for comparing mandibular shape asymmetry in patients with skeletal Class I and skeletal Class III patterns in a group level. In clinical scenarios, a small amount of asymmetry in certain patients is probably normal. For example, an asymmetric-shaped mandible could compensate for an asymmetric maxilla or cranial base. Further analysis would link treatment planning and outcome evaluation in specific asymmetry patients.

CONCLUSIONS

In conclusion, this study describes an automatic method for quantifying mandibular shape asymmetry in 3D, which overcomes the projection distortion problems inherent in 2D measurements and provides more comprehensive asymmetry information than conventional linear distance and angular measurement in 3D. Precise quantification of mandibular asymmetry will aid orthodontists and surgeons to better understand the issue of asymmetry and guide treatment planning. In addition, the fully automatic pipeline includes automatically segmenting the mandible from CBCT images and automatically identifying spatially-dense landmarks on the mandibular surface, which will benefit large-scale image analysis.

AUTHOR CREDIT STATEMENT

Yi Fan contributed to conceptualization, analysis, and original draft preparation; Yungeng Zhang contributed

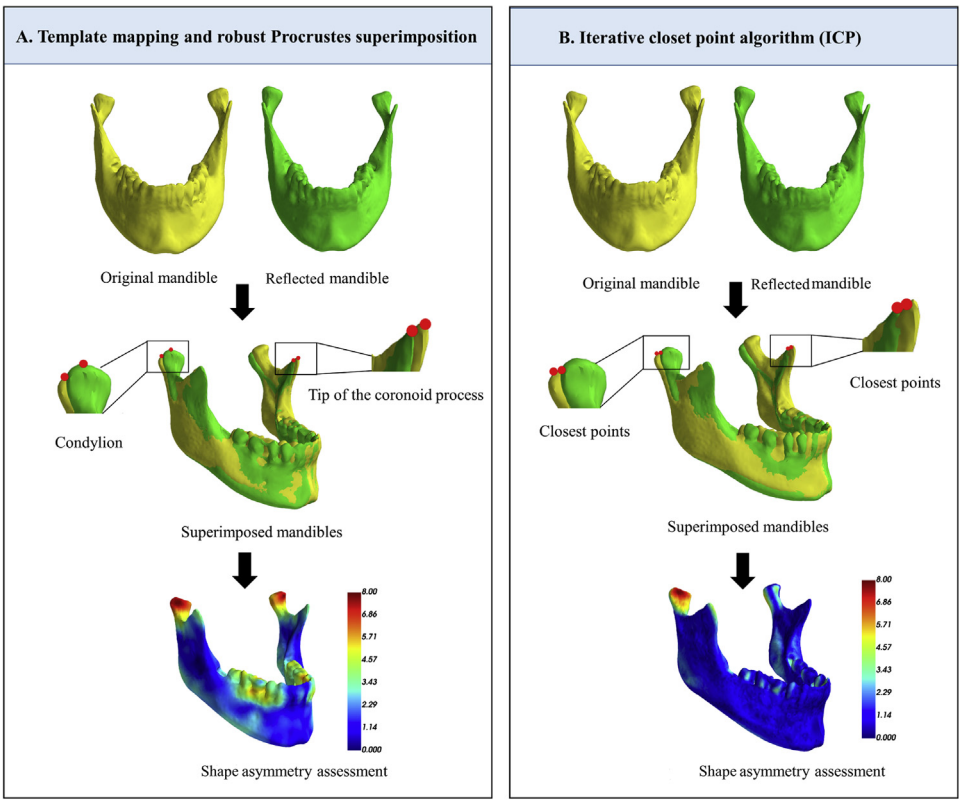

Fig 7. Mandibular shape asymmetry assessment: **A,** The corresponding points are established onto each paired original and reflected mandible by template mapping. The robust Procrustes superimposition is used to superimpose the original and reflected mandible on the basis of the correspondence. The difference between the original and mirror mandible at each point is graphically visualized and quantified by color maps, indicating the location of asymmetry; **B,** The iterative closest-point algorithm approximates corresponding points based on the closest neighbor on the surface instead of anatomic meaningful correspondence, which fails to quantify severe shape asymmetry.

to data analysis; Yuru Pei contributed to manuscript review; Hongbin Zha contributed to manuscript review; Wei He contributed to the data collection and original draft preparation; Gui Chen contributed to the data collection and original draft preparation; Guangying Song contributed to manuscript review; Anthony Penington contributed to conceptualization and manuscript review; Nicky Kilpatrick contributed to conceptualization; Paul Schneider contributed to manuscript review; Harold Matthews contributed to manuscript review and editing; Peter Claes contributed to manuscript review and editing; Ruoping Jiang contributed to manuscript review and editing; Tianmin Xu contributed to manuscript review and editing.

REFERENCES

1. Solem RC, Ruellas A, Ricks-Oddie JL, Kelly K, Oberoi S, Lee J, et al. Congenital and acquired mandibular asymmetry: mapping growth and remodeling in 3 dimensions. Am J Orthod Dentofacial Orthop 2016;150:238-51.
2. Kearns GJ, Padwa BL, Mulliken JB, Kaban LB. Progression of facial asymmetry in hemifacial microsomia. Plast Reconstr Surg 2000; 105:492-8.
3. Chia MS, Naini FB, Gill DS. The aetiology, diagnosis and management of mandibular asymmetry. Orthodontic Update 2008;1:44-52.
4. Ramirez-Yañez GO, Stewart A, Franken E, Campos K. Prevalence of mandibular asymmetries in growing patients. Eur J Orthod 2011; 33:236-42.
5. Pinto AS, Buschang PH, Throckmorton GS, Chen P. Morphological and positional asymmetries of young children with functional unilateral posterior crossbite. Am J Orthod Dentofacial Orthop 2001; 120:513-20.
6. Fong JH, Wu HT, Huang MC, Chou YW, Chi LY, Fong Y, et al. Analysis of facial skeletal characteristics in patients with chin deviation. J Chin Med Assoc 2010;73:29-34.
7. Shah SM, Joshi MR. An assessment of asymmetry in the normal craniofacial complex. Angle Orthod 1978;48:141-8.
8. Ferrario VF, Sforza C, Poggio CE, Tartaglia G. Distance from symmetry: a three-dimensional evaluation of facial asymmetry. J Oral Maxillofac Surg 1994;52:1126-32.

9. Lam PH, Sadowsky C, Omerza F. Mandibular asymmetry and condylar position in children with unilateral posterior crossbite. Am J Orthod Dentofacial Orthop 1999;115:569-75.
10. Major PW, Johnson DE, Hesse KL, Glover KE. Effect of head orientation on posterior anterior cephalometric landmark identification. Angle Orthod 1996;66:51-60.
11. Lee H, Bayome M, Kim SH, Kim KB, Behrents RG, Kook YA. Mandibular dimensions of subjects with asymmetric skeletal Class III malocclusion and normal occlusion compared with cone-beam computed tomography. Am J Orthod Dentofacial Orthop 2012; 142:179-85.
12. Thiesen G, Freitas MPM, Araújo EA, Gribel BF, Kim KB. Three-dimensional evaluation of craniofacial characteristics related to mandibular asymmetries in skeletal Class I patients. Am J Orthod Dentofacial Orthop 2018;154:91-8.
13. Cao HL, Kang MH, Lee JY, Park WJ, Choung HW, Choung PH. Quantification of three-dimensional facial asymmetry for diagnosis and postoperative evaluation of orthognathic surgery. Maxillofac Plast Reconstr Surg 2020;42:17.
14. Duran GS, Dindaroğlu F, Kutlu P. Hard- and soft-tissue symmetry comparison in patients with Class III malocclusion. Am J Orthod Dentofacial Orthop 2019;155:509-22.
15. Çiçek Ö, Abdulkadir A, Lienkamp SS, Brox T, Ronneberger O. U-net: learning dense volumetric segmentation from sparse annotation. In: International Conference on Medical Image Computing and Computer-Assisted Intervention. Cham, Switzerland: Springer International Publishing; 2016. p. 424-32.
16. Cevidanes LHS, Alhadidi A, Paniagua B, Styner M, Ludlow J, Mol A, et al. Three-dimensional quantification of mandibular asymmetry through cone-beam computerized tomography. Oral Surg Oral Med Oral Pathol Oral Radiol Endod 2011;111: 757-70.
17. Yatabe M, Garib D, Faco R, de Clerck H, Souki B, Janson G, et al. Mandibular and glenoid fossa changes after bone-anchored maxillary protraction therapy in patients with UCLP: a 3-D preliminary assessment. Angle Orthod 2017;87:423-31.
18. White JD, Ortega-Castrillón A, Matthews H, Zaidi AA, Ekrami O, Snyders J, et al. MeshMonk: open-source large-scale intensive 3D phenotyping. Sci Rep 2019;9:6085.
19. Fan Y, Penington A, Kilpatrick N, Hardiman R, Schneider P, Clement J, et al. Quantification of mandibular sexual dimorphism during adolescence. J Anat 2019;234:709-17.
20. Fan Y, Schneider P, Matthews H, Roberts WE, Xu T, Wei R, et al. 3D assessment of mandibular skeletal effects produced by the Herbst appliance. BMC Oral Health 2020;20:117.
21. Verhelst PJ, Matthews H, Verstraete L, Van der Cruyssen F, Mulier D, Croonenborghs TM, et al. Automatic 3D dense phenotyping provides reliable and accurate shape quantification of the human mandible. Sci Rep 2021;11:8532.
22. Thiesen G, Gribel BF, Kim KB, Pereira KCR, Freitas MPM. Prevalence and associated factors of mandibular asymmetry in an adult population. J Craniofac Surg 2017;28:e199-203.
23. Severt TR, Proffit WR. The prevalence of facial asymmetry in the dentofacial deformities population at the University of North Carolina. Int J Adult Orthodon Orthognath Surg 1997;12:171-6.
24. Sezgin OS, Celenk P, Arici S. Mandibular asymmetry in different occlusion patterns. Angle Orthod 2007;77:803-7.
25. Fan Y, Beare R, Matthews H, Schneider P, Kilpatrick N, Clement J, et al. Marker-based watershed transform method for fully automatic mandibular segmentation from CBCT images. Dentomaxillofac Radiol 2019;48:20180261.
26. Kainmueller D, Lamecker H, Seim H, Zinser M, Zachow S. Automatic extraction of mandibular nerve and bone from cone-beam CT data. Med Image Comput Assist Interv 2009;12:76-83.
27. Wang L, Chen KC, Gao Y, Shi F, Liao S, Li G, et al. Automated bone segmentation from dental CBCT images using patch-based sparse representation and convex optimization. Med Phys 2014; 41:043503.
28. Wang L, Gao Y, Shi F, Li G, Chen KC, Tang Z, et al. Automated segmentation of dental CBCT image with prior-guided sequential random forests. Med Phys 2016;43:336.
29. Ercan I, Ozdemir ST, Etoz A, Sigirli D, Tubbs RS, Loukas M, et al. Facial asymmetry in young healthy subjects evaluated by statistical shape analysis. J Anat 2008;213:663-9.
30. Ferrario VF, Sforza C, Miani A, Serrao G. Dental arch asymmetry in young healthy human subjects evaluated by Euclidean distance matrix analysis. Arch Oral Biol 1993;38:189-94.
31. Claes P, Walters M, Vandermeulen D, Clement JG. Spatially-dense 3D facial asymmetry assessment in both typical and disordered growth. J Anat 2011;219:444-55.
32. Xiong Y, Zhao Y, Yang H, Sun Y, Wang Y. Comparison between interactive closest point and Procrustes analysis for determining the median sagittal plane of three-dimensional facial data. J Craniofac Surg 2016;27:441-4.